Results in Applied Mathematics 10 (2021) 100153

Contents lists available at ScienceDirect

Results in Applied Mathematics

journal homepage: www.elsevier.com/locate/results-in-applied-mathematics

Dynamics analysis of typhoid fever with public health education programs and final epidemic size relation

Salihu Sabiu Musa [a,b], Shi Zhao [a,c,d], Nafiu Hussaini [e], Salisu Usaini [b], Daihai He [a,*]

[a] Department of Applied Mathematics, Hong Kong Polytechnic University, Hong Kong, China
[b] Department of Mathematics, Kano University of Science and Technology, Wudil, Nigeria
[c] JC School of Public Health and Primary Care, Chinese University of Hong Kong, Hong Kong, China
[d] Shenzhen Research Institute of Chinese University of Hong Kong, Shenzhen, China
[e] Department of Mathematical Sciences, Bayero University, Kano, Nigeria

ARTICLE INFO

Article history:
Received 14 February 2021
Received in revised form 2 March 2021
Accepted 7 March 2021
Available online 1 April 2021

Keywords:
Typhoid fever
Reproduction number
Stability analysis
Sensitivity analysis
Final size relation

ABSTRACT

In this paper, an epidemic model is develop and use to investigate the transmission dynamics of the typhoid fever epidemic (TF, a bacterial infection caused by *Salmonella serotype Typhi bacteria*). The model assesses the impact of public health education programs (PHEP) on reducing the pathogenesis of TF which can cause large outbreaks especially in resource-poor settings. The model is fitted well to the data for TF cases for Taiwan, China. Results from our mathematical analysis reveal that the disease-free equilibrium (DFE) of the model is globally asymptotically stable (GAS) when the basic reproduction number ($\mathcal{R}_0$) is below or equal to unity, and unstable when it is above unity. Further analysis also shows that the endemic equilibrium (EE) of the model is GAS whenever the $\mathcal{R}_0$ is above unity with some certain conditions , indicating the potential for the TF to spread and cause outbreaks in the community. We obtain a final size relation with consideration of human-to-human transmission route that could be used to report the actual size of the outbreaks over the cause of the epidemic period. Furthermore, sensitivity analysis results reveal the most sensitive parameters that are vital to combat the TF epidemic in Taiwan. Also, a wavelets analysis is performed to explore significant periodicities of the TF outbreaks in Taiwan, China.

1. Introduction

Typhoid fever (TF), a life-threatening disease or infection, that is caused by the bacterium *Salmonella Typhi* and is transmitted via contaminated food items or water [1]. The TF disease is still a serious challenge to global public health, causing about 10–20 million new infections and more than a quarter-million deaths annually mostly in Africa [1–3]. The disease incidence is largely reduced especially in developed countries due to the clean water supply and good sewage systems, indicating that poor drainage systems and lack of water quality control contributes largely to the new infections [2]. Although the TF disease is curable, however the increasing resistance to different types of antibiotics make the disease's treatment more intricate [1]. Three major types of TF vaccines currently recommended by the World Health Organization (WHO) are: (i) an injectable typhoid conjugate vaccine (TCV), (ii) an injectable unconjugated polysaccharide vaccine based on the purified Vi antigen (also called Vi-PS vaccine), and (iii) an oral live-attenuated Ty21a vaccine in capsule formulation [1]. Besides, the WHO further recommends that all control programs of TF should be implemented,

* Corresponding author.
E-mail address: daihai.he@polyu.edu.hk (D. He).

https://doi.org/10.1016/j.rinam.2021.100153

those include water quality and sanitation improvements, public health education/awareness campaigns, and training and re-training of health workers in diagnostic testing and proper treatment [1].

Several epidemic models have been proposed (designed) and used to capture qualitative acumen or knowledge into the dynamics features of infectious diseases in a community, see, for instance, [4–11], however these previous studies have been elongated over time to incorporates different aspect related to infectious diseases dynamics, such as the influence of human behavior such as influence of human behavior [12–15], impact of limited medical resources [16–21], public health education programs [22–28], etc., several mechanistic modeling studies have been done to explore the dynamics transmission of TF disease, some of which have considered direct transmission route (human to human) only [29,30], while others considered indirect transmission route (environment to human) only [3].

To our knowledge, none of the previous studies have considered both direct and indirect transmission routes coupled with public health education programs to assess the dynamics of TF transmission. In the current study, we consider both human to human and environment to human transmission routes together with the public health education programs as a separate compartment to understand and reveal more qualitative insight into the transmission dynamics of TF. Further, as motivated by the aforementioned studies, in particular, we adopted the recent work of Yang et al. [27] which investigated the impact of public awareness programs on the dynamics of cholera, we incorporated the compartment which represents public health education programs (that include house to house enlightenment programs, media-coverage, reports, etc.) to assess its impact and to provide an effective suggestion for the control strategy to combat TF in the endemic areas. Furthermore, using the approach as in [31] we obtained a wavelet results (depicted in Fig. B.1) to shows the temporal patterns of TP outbreaks in Taiwan, to get more insight and understanding into the dynamics patterns of the TP epidemic in Taiwan. We found that the local periodicity of the typhoid cases indicates a significant periodicity that needs urgent consideration for effective control and mitigation for the TP outbreaks.

The proposed model is described in Section 2 and examined in Section 3. The final epidemic size relation is computed in Section 4. We present numerical simulation results in Section 5.

2. Description of the typhoid fever model

Here, an epidemic model was designed to study the dynamics of TF transmission in a community. The model incorporates both direct (human to human) and indirect (environment to human) route of transmission coupled with public health education programs as a separate compartment (adopted from the work of Yang et al. [27]). The total human population size, denoted by N, is split into sub-populations (see Table 1 for summaries): Susceptible (S), infected (I), carriers (C), and recovered (R), so that $N = S + I + C + R$. Also, let B represent the bacteria concentration available in the environment, and A the number or density of public health education programs (such as house to house visit, social media enlightenment programs, training of health professionals in diagnosis and treatment, and reports) driven by the prevalence of the disease and media coverage.

Susceptible humans (S) are infected either by effective contact with infected individuals (direct transmission) or interact with contaminated environment (indirect transmission). The population of susceptible individuals can be reduced by natural death at a rate μ (all humans compartments are assumed to suffer same natural death). The infected individuals (I), either progress to carrier class C, at a rate σ or recover at a rate τ_1. Individuals in the C class can recover at a rate τ_2 (note that $\tau_1 < \tau_2$) [3]. Infectious individuals from both I and C classes excrete the bacteria into the environment with the fact that the excretion from the I class at a rate θ_1 is substantially higher than those by the C class at a rate θ_2, this is because of the long period taken by the C class without showing any symptoms/sickness of the typhoid. The parameter δ measure the disease induced death rate from the I class, ψ is the rate of waning immunity, K parameter denotes half saturation of bacteria concentration, υ measure the removal rate of bacteria from the environment. The parameter α ($0 < \alpha < 1$) is the modification parameter which shows that I seems more likely to transfer typhoid infection than C, and also infection from I is significantly higher than infection from C [3]. The number of public health education programs (awareness programs) grows with an influx ξ and simulated by the prevalence of the disease at a rate η, and decays at a rate γ. We assume that β_1, β_2, θ_1, and θ_2 are explicitly dependent on A, also they decrease with the increase of A, indicating the impact of public health education programs on the transmission dynamics of typhoid fever. Therefore, the above mentioned assumptions of the model for the typhoid fever disease results in the following system of nonlinear ordinary differential equations.

$$\begin{cases} \dfrac{dS}{dt} = \pi + \psi R - \beta_1(A)(I + \alpha C)S - \beta_2(A)\dfrac{B}{B+K}S - \mu S, \\ \dfrac{dI}{dt} = \beta_1(A)(I + \alpha C)S + \beta_2(A)\dfrac{B}{B+K}S - (\mu + \delta + \sigma + \tau_1)I, \\ \dfrac{dC}{dt} = \sigma I - (\mu + \tau_2)C, \\ \dfrac{dR}{dt} = \tau_1 I + \tau_2 C - (\mu + \psi)R, \\ \dfrac{dB}{dt} = \theta_1(A)I + \theta_2(A)C - \upsilon B, \\ \dfrac{dA}{dt} = \xi + \eta\dfrac{I + \alpha C}{N} - \gamma A. \end{cases} \tag{2.1}$$

Table 1
Parameters interpretation of the model (2.1).

Parameter	Interpretation
π	Recruitment rate
ψ	Immunity wanning rate
β_1	Human to human infection rate
β_2	Environment to human infection rate
α	Modification parameter
μ	Natural death rate
σ	Progression rate from I to C
δ	Disease induced death rate
θ_1	Bacteria excretion rate from I
θ_2	Bacteria excretion rate from C
γ	Decay rate of PHEP
υ	Bacteria decay/removal rate
ξ	Influx rate of PHEP
η	Simulating rate of PHEP
τ_1	Rate of recovery from I compartment
τ_2	Rate of recovery from C compartment
K	Half saturation concentration of bacteria

The following items presents some of the main assumptions used in the description of the model (2.1):

(**i**) $\beta_1(A)$, $\beta_2(A)$, $\theta_1(A)$ and $\theta_2(A)$ are continuously differentiable functions;
(**ii**) $\beta_1(A)$, $\beta_2(A)$, $\theta_1(A)$ and $\theta_2(A)$ are positive functions on $[0, A_{max}]$;
(**iii**) $\beta_1'(A) \leq 0$, $\beta_2'(A) \leq 0$, $\theta_1'(A) \leq 0$ and $\theta_2'(A) \leq 0$,

where $A_{max} = \frac{\xi+\eta(1+\alpha)}{\gamma}$, and '$\prime$' is the derivative with respect to A. Note that the analysis is perform using the autonomous version of the model for computational conveniences.

2.1. Basic properties

Following a standard comparison theorem [32], we have $B^0 \leq B \leq B_{max}$ and $A^0 \leq A \leq A_{max}$, where $B_{max} = \frac{(\theta_1(0)+\theta_2(0))N}{\upsilon}$ and $A_{max} = \frac{\xi+\eta(1+\alpha)}{\gamma}$. Hence, we have the following biologically feasible region/domain

$$\Omega = \left\{(S, I, C, R, B, A) \in \mathbb{R}_+^6 : S + I + C + R = N, B^0 \leq B \leq B_{max}, A^0 \leq A \leq A_{max}\right\}.$$

Obviously, all solutions of the model (2.1) that starts in Ω, remain in the that region for all positive time, i.e., $t \geq 0$. So that, Ω is positive-invariant, and therefore, it is enough to evaluate solutions confined in Ω. Hence, the usual existence, uniqueness and continuation results hold for the model (2.1) in Ω [33,34].

3. Model analysis

3.1. Disease-free equilibrium, DFE

The DFE of the system (2.1), given by

$$E^0 = (S^0, I^0, C^0, R^0, B^0, A^0) = (\frac{\pi}{\mu}, 0, 0, 0, 0, \frac{\xi}{\gamma}),$$

is always feasible. Local stability of E^0 can be computed in terms of $\mathcal{R}_0$ which represent the number of infected individuals to be obtained if one infected individual is introduced into a completely susceptible population of humans [34–39].

3.2. Basic reproduction number, $\mathcal{R}_0$

It can be shown here, using the next generation matrix (NGM) [35,37], that, the associated reproduction number of the system (2.1) (represented by $\mathcal{R}_0 = \rho(FV^{-1})$, where ρ denotes the spectral radius of the NGM, FV^{-1}) is as below. The matrix F denotes the new infection terms, and the other terms of the model is represented by the matrix V, and are given, respectively, by:

$$F = \begin{bmatrix} a_1 & a_2 & a_3 \\ 0 & 0 & 0 \\ 0 & 0 & 0 \end{bmatrix}, \quad \text{and} \quad V = \begin{bmatrix} Q_1 & 0 & 0 \\ -\sigma & Q_2 & 0 \\ -b_1 & -b_2 & \upsilon \end{bmatrix}. \tag{3.1}$$

Where, $N^0 = \frac{\pi}{\mu} = S^0$, $a_1 = \frac{\beta_1(A^0)\pi}{\mu}$, $a_2 = \frac{\beta_1(A^0)\alpha\pi}{\mu}$, $a_3 = \frac{\beta_2(A^0)\pi}{\mu K}$, $b_1 = \theta_1(A^0)$, $b_2 = \theta_2(A^0)$, $Q_1 = \mu + \delta + \sigma + \tau_1$, $Q_2 = \mu + \tau_2$, and $Q_3 = \mu + \psi$. Therefore, the $\mathcal{R}_0$ is given in Eq. (3.2) below

$$\mathcal{R}_0 = \frac{a_1 Q_2 + a_2\sigma}{Q_1 Q_2} + \frac{a_3\sigma b_2 + a_3 Q_2 b_1}{Q_1 Q_2 \upsilon} = \mathcal{R}_h + \mathcal{R}_e. \tag{3.2}$$

The threshold quantity, $\mathcal{R}_0$, is epidemiologically interpreted as follows. The two terms in Eq. (3.2) are respectively interpreted as follows;

i. the first part, $\mathcal{R}_h$, represents direct transmission reproduction number,
ii. and the second part, $\mathcal{R}_e$, represents indirect transmission reproduction number.

Let $\mathcal{R}_0^*$ denotes the reproduction number in absence of public health education (i.e., we let $\beta_1(A) = \beta_1(0)$, $\beta_2(A) = \beta_2(0)$, $\theta_1(A) = \theta_1(0)$ and $\theta_2(A) = \theta_2(0)$). Thus,

$$\mathcal{R}_0^* = \frac{a_1^0 Q_2 + a_2^0\sigma}{Q_1 Q_2} + \frac{a_3^0\sigma b_2^0 + a_3^0 Q_2 b_1^0}{Q_1 Q_2 \upsilon}, \tag{3.3}$$

where, $a_1^0 = \frac{\beta_1(0)\pi}{\mu}$, $a_2^0 = \frac{\beta_1(0)\alpha\pi}{\mu}$, $a_3^0 = \frac{\beta_2(0)\pi}{\mu K}$, $b_1^0 = \theta(0)$, $b_2^0 = \theta_2(0)$. According to our assumptions, it is easy to see that $\mathcal{R}_0 \leq \mathcal{R}_0^*$, which shows that the presence of public health education programs will diminished the risk of TF prevalence. The LAS result given below follows from Theorem 2 of [37].

Theorem 3.1. *Consider the region, Ω, the DFE, E^0, of the model given in Eq. (2.1), is LAS if $\mathcal{R}_0$ is below unity, and unstable if $\mathcal{R}_0$ above unity.*

3.3. Equilibrium analysis

In this sub-section, we analyzed the equilibria of the system (2.1), in order to get more qualitative insights into the transmission dynamics of the TF disease.

Let

$$E^* = (S, I, C, R, B, A)$$

be an endemic equilibrium, EE, of the system (2.1), which satisfies the system of eqns given below

$$\begin{cases} \pi + \psi R - \beta_1(A)(I + \alpha C)S - \beta_2(A)\dfrac{B}{B+K}S - \mu S = 0, \\ \beta_1(A)(I + \alpha C)S + \beta_2(A)\dfrac{B}{B+K}S - (\mu + \delta + \sigma + \tau_1)I = 0, \\ \sigma I - (\mu + \tau_2)C = 0, \\ \tau_1 I + \tau_2 C - (\mu + \psi)R = 0, \\ \theta_1(A)I + \theta_2(A)C - \upsilon B = 0, \\ \xi + \eta\dfrac{I + \alpha C}{N} - \gamma L = 0, \end{cases} \tag{3.4}$$

which implies that,

$$\begin{cases} S = \dfrac{Q_1 I}{\beta_1(A) I n + \beta_2(A)\frac{B}{B+K}}, \\ C = \dfrac{\sigma I}{Q_2}, \\ R = \dfrac{(\tau_1 Q_2 + \tau_2\sigma)I}{Q_2 Q_3}, \\ B = \dfrac{(\theta_1(A)Q_2 + \theta_2(A)\sigma)I}{Q_2\upsilon}, \\ A = \dfrac{\xi}{\gamma} + \dfrac{\eta(Q_2 + \alpha\sigma)I}{Q_3\gamma} := G_0(I), \end{cases} \tag{3.5}$$

where $n = (1 + \frac{\alpha\sigma}{Q_2})$.

Now, since $N = S + I + C + R$, we have

$$S = N - mI := G_1(I), \tag{3.6}$$

with $m = 1 + \frac{\sigma}{Q_2} + \frac{(\tau_1 Q_2 + \tau_2\sigma)}{Q_2 Q_3}$.

Also, from the first equation of model (3.4), we have

$$S = \frac{Q_1}{H(I)} := G_2(I), \tag{3.7}$$

where

$$H(I) = \beta_1(G_0(I))n + \frac{\beta_2(G_0(I))[Q_2\theta_1(G_0(I)) + \sigma\theta_2(G_0(I))]}{[Q_2\theta_1(G_0(I)) + \sigma\theta_2(G_0(I))]I + KQ_2v},$$

which implies that

$$H'(I) = \frac{H_1(I) + H_2(I) + H_3(I)}{[I(Q_2\theta_1(G_0(I)) + \sigma\theta_2(G_0(I))) + K]^2},$$

with

$H_1(I) = G_0'(I)(Q_2\theta_1'(G_0(I)))$,
$H_2(I) = \sigma\theta_2'(G_0(I))(I(Q_2\theta_1(G_0(I)) + \sigma\theta_2(G_0(I))) + K) \cdot \beta_2'(G_0(I)) \cdot [Q_2\theta_1(G_0(I)) + \sigma\theta_2(G_0(I))]$,
$H_3(I) = \beta_2(G_0(I))(Q_2\theta_1(G_0(I)) + \sigma\theta_2(G_0(I))) \cdot (I(Q_2\theta_1'(G_0(I))G_0'(I) + \sigma\theta_2'(G_0(I))G_0'(I)) + Q_2\theta_1(G_0(I)) + \sigma\theta_2(G_0(I)))$, where the " $'$ " denote the derivative with respect to t.

Therefore, the intersection of the two curves $S = G_1(I)$ and $S = G_2(I)$ in $\mathbb{R}^2_+$ determine the nontrivial disease free equilibria. Therefore, since $G_0'(I) = \frac{\eta(Q_2+\alpha\sigma)}{Q_3\gamma} > 0$ which shows that $H'(I) \leq 0$. Thus,

i. $G_1(I)$ is strictly decreasing function of I; and
ii. $G_2(I)$ is non-decreasing function of I.

Hence, it can be verified that $G_1(0) = N$, $G_2(0) = \frac{N}{\mathcal{R}_0}$, $G_1(\frac{N}{m}) = 0$, and $G_2(\frac{N}{m}) > 0$.

Therefore, we have

(a_1) If $\mathcal{R}_0 > 1$, the curves $S = G_1(I)$ and $S = G_2(I)$ have a unique intersection lying in the interior of $\mathbb{R}^2_+$, due to the fact that $S = G_2(0) < S = G_1(0)$. Therefore, at this intersection point, Eq. (3.5) gives $C, R, B > 0$ (since $I > 0$).
(a_2) If $\mathcal{R}_0 \leq 1$, the curves $S = G_1(I)$ and $S = G_2(I)$ have no intersection in the interior of $\mathbb{R}^2_+$ due to the fact that $G_2(0) \geq G_1(0)$.

Therefore, Eq. (3.4) shows that the system (2.1) permits a unique equilibrium, i.e., the E^0, if $\mathcal{R}_0 \leq 1$; and also accepts two equilibria, i.e., the E^0 and an endemic equilibrium if $\mathcal{R}_0 > 1$.

Now, following a standard comparison theorem [32], we have $B^0 \leq B \leq B_{max}$ and $A^0 \leq A \leq A_{max}$, where $B_{max} = \frac{[\theta_1(0)+\theta_2(0)]N}{v}$ and $A_{max} = \frac{\xi+\eta(1+\alpha)}{\gamma}$. Hence, we have the following biologically feasible region/domain

$$\Omega = \left\{(S, I, C, R, B, A) \in \mathbb{R}^6_+ : S + I + C + R = N, B^0 \leq B \leq B_{max}, A^0 \leq A \leq A_{max}\right\}.$$

Theorem 3.2. *The following statements hold for system (2.1),*

(1) If $\mathcal{R}_0 \leq 1$, the continuum DFE, E^0, is GAS in Ω;
(2) If $\mathcal{R}_0 > 1$, the E^0 is unstable and there exists a unique EE, i.e., $E^* = (S^*, I^*, C^*, R^*, B^*, A^*) \in int(\Omega)$, where $int(\Omega)$ is the interior of Ω. Additionally, the system (1) is uniformly persistent, i.e., $\liminf_{t\to\infty} (\boldsymbol{I(t), B(t)}) \geqslant (c, c)$ for some $c > 0$, with the initial condition in the interior of Ω, denoted by Ω^0.

Proof. Let $p = (I, C, B)^T$ and $q = (S, R, A)$. Obviously, $\frac{dx}{dt} \leq (F - V)p$, where the matrices F and V are given in Eq. (3.1). Let $g = (a_1 + \frac{a_2\sigma}{Q_2}, 0, a_3)$, where g is the left eigenvector associated with the eigenvalue $\mathcal{R}_0$ of the matrix $V^{-1}F$. So that, $gV^{-1}F = \mathcal{R}_0 * g$.

Define a Lyapunov function given by $U = gV^{-1}p$. Now, differentiating U along a solution of Eq. (2.1), where the "$\prime$" denotes the derivative with respect to time, implies $U' = gV^{-1}p' \leq gV^{-1}(F - V)p = g(\mathcal{R}_0 - 1)p$.

Now, we consider the following three cases.

(i) $\mathcal{R}_0 < 1$. The strict equality $U' = 0$ holds, implies that $gp = 0$. By taking the positive part of g, we have $I = C = B = 0$, so that when $\mathcal{R}_0 < 1$ equation (2.1) yields $S = S^0$, $A = A^0$, and $I = C = B = R = 0$. Hence, the invariant set on which $U' = 0$ contains only one point which is the E^0.

(ii) if $\mathcal{R}_0 = 1$, the equality $U' = 0$ implies $\beta_1(A)(I + \alpha C)S = a_1(I + \alpha C)$, $\beta_2(A)\frac{B}{B+K}S = a_3B$, $\theta_1(A) = b_1$ and $\theta_2(A) = b_2$. Thus, either $(C1)$ $I = C = B = 0$ or $(C2)$ $B = 0$, $\beta_1(A) = \beta_1(A^0)$ and $\beta_2(A) = \beta_2(A^0)$. Therefore, if $(C1)$ holds, then the system (2.1) gives $S = S^0$, $R = 0$ and $A = A^0$. Similarly, when $(C2)$ holds, then we have $I = C = B = 0$, which is similar to the condition $(C1)$. Hence, the largest invariant set on which U' is the singleton set $E^0 = \left(\frac{\pi}{\mu}, 0, 0, 0, 0, \frac{\xi}{\gamma}\right)$.

(iii) For $\mathcal{R}_0 > 1$. Following [40–42] and the continuity of vector field, so that $U' > 0$ in a neighborhood of the E^0 in Ω^0. Hence, by Lyapunov theory of stability, the E^0 is unstable.

3.3.1. Global stability analysis of the EE

Here, we consider θ_1 and θ_2 be constant, then the following result is obtained.

Theorem 3.3. *The EE, E^*, is GAS in Ω^0 when $\mathcal{R}_0 > 1$ provided that*

$$\left(1-\frac{\beta_1 I}{\beta_1^* I^*}\right)\left(1-\frac{B\beta_1^* I^*}{B^*\beta_1 I}\right)\geq 0, \tag{3.8}$$

$$\left(1-\frac{\beta_1 C}{\beta_1^* C^*}\right)\left(1-\frac{C\beta_1^* C^*}{C^*\beta_1 C}\right)\geq 0, \tag{3.9}$$

and

$$\left(1-\frac{\beta_2\left(\frac{B}{B+K}\right)}{\beta_2^*\left(\frac{B^*}{B^*+K}\right)}\right)\left(1-\frac{C\frac{\beta_2^* B^*}{B^*+K}}{C^*\frac{\beta_2 B}{B+K}}\right)\geq 0. \tag{3.10}$$

For the proof of the above theorem of the global stability of the EE, see Appendix A.

4. Final epidemic size relation

The final size relation is a relation is computed in this part, i.e., the $\mathcal{R}_0$ and the number of individuals who remain in each disease-free epidemiological compartment during the epidemic period [43]. We obtained the final epidemic size relation for the reduced (a special version of the model) model (2.1) (i.e., human-to-human transmission only) [43,44]. We assumed that $\pi = \mu = \psi = 0$, that is, the final size is calculated within a short period in order to report the (nearly) actual outbreaks of the disease over the cause of the epidemic. The reduced model (with human-to-human transmission route only) is given by the following nonlinear ODEs.

$$\begin{cases} \dfrac{dS}{dt} = -\beta_1(A)(I+\alpha C)S, \\ \dfrac{dI}{dt} = \beta_1(A)(I+\alpha C)S-(\delta+\sigma+\tau_1)I, \\ \dfrac{dC}{dt} = \sigma I-\tau_2 C, \\ \dfrac{dR}{dt} = \tau_1 I+\tau_2 C, \\ \dfrac{dA}{dt} = \xi+\eta\dfrac{I+\alpha C}{N}-\gamma A, \end{cases} \tag{4.1}$$

where the basic reproduction number of the reduced model (4.1) is given by $\mathcal{R}_0^{**} = \frac{\beta_1 S_0(\alpha\sigma+\tau_2)}{\tau_2(\delta+\sigma+\tau_1)}$.

Integrating the system (4.1) from 0 to ∞, so that

$$N - S_\infty = \delta\int_0^\infty I\,dt. \tag{4.2}$$

Also, integrating the third equation of (4.1) we obtain

$$\sigma\int_0^\infty I\,dt = \tau_2\int_0^\infty C\,dt - C_0. \tag{4.3}$$

From the first equation of (4.1), we have

$$\ln\frac{S_0}{S_\infty} = \beta_1(A)\int_0^\infty I\,dt + \beta_1(A)\alpha\int_0^\infty C\,dt. \tag{4.4}$$

Substituting Eqs. (4.2) and (4.3) into Eq. (4.4), we have

$$\begin{aligned} \ln\frac{S_0}{S_\infty} &= \beta_1(A)\int_0^\infty I\,dt + \beta_1(A)\frac{\alpha\sigma}{\tau_2}\int_0^\infty I\,dt + \beta_1(A)\frac{\alpha C_0}{\tau_2} \\ &= \beta_1(A)\left(1+\frac{\alpha\sigma}{\tau_2}\right)\int_0^\infty I\,dt + \beta_1(A)\frac{\alpha C_0}{\tau_2} \\ &= \frac{\beta_1(A)N(\alpha\sigma+\tau_2)}{\delta\tau_2}\left(1-\frac{S_\infty}{N}\right)+\beta_1(A)\alpha\frac{C_0}{\tau_2} \\ &= \frac{\mathcal{R}_0^{**}(\delta\sigma+\tau_1)}{\delta}\left(1-\frac{S_\infty}{N}\right)+\beta_1(A)\alpha\frac{C_0}{\tau_2}. \end{aligned} \tag{4.5}$$

Table 2
Baseline values of the model parameters.

Parameter	Baseline [Range]	Units	Source
π	813.5433	persons per day	[3]
ψ	0.0013 [1, 1]	per day	[30]
β_1	1.57×10^{-5}	per day	Estimated [29]
β_2	1.97×10^{-5}	per day	Calculated [29]
α	3×10^{-4}	per day	Assumed
μ	3.717×10^{-5}	per day	[3]
σ	0.04 [0.03, 0.05]	per day	[3,29]
δ	0.0025	per day	Calculated [3,29]
θ_1	10	dimensionless	[3]
θ_2	1	dimensionless	[3]
γ	0.033	per day	Estimated, [27]
υ	0.0345	per day	[3]
ξ	0.1	per day	Estimated [27]
η	2	(cellml^{-1} humans^{-1}) per day	Estimated [45]
τ_1	0.0357	per day	[3]
τ_2	3.2×10^{-4}	per day	Calculated [29]
K	10^6	(cells $\times$ ml^{-1}) per day	Estimated [27]

Hence, the final size relation of the system (4.1) is given by Eq. (4.5). Note that the zero subscripts in the state variables indicate the initial value of the state.

5. Numerical simulations

5.1. Model fitting

In this sub-section, the autonomous model version of the model (2.1) was fitted to the cumulative number of yearly cases of the reported TF scenario in Taiwan from 2009–2018. The TF case data were fitted using Pearson's Chi-square and the least square techniques [33]. The R statistical software version 3.4.1 or above was used for the simulation processes. The time series TF cases were obtained from Taiwan National Infectious Disease Statistics System [46]. The demographic quantities were obtained from the World Bank population website [47]. Other demographic parameters (i.e., recruitment rate, π, and natural death rate, μ) were calculated as follows; the average population and life expectancy in Taiwan is 23 373 000 and 78.712 years, respectively [48]. Thus, the expression for μ is given by $\mu^{-1} = 78.712$ years. Hence, $\frac{\pi}{\mu} = 23\,373\,000$, which implies that $\pi = 813.5433$ day^{-1}. It is worth noting that all the remaining parameters are fixed as given in Table 2. Thus, the fitting results was depicted in Fig. 1. Note also that the fitting scenario was done for an illustrative purpose (for model validation purpose), thus we choose a small portion from the given population of approximately 23 million in Taiwan.

5.2. Sensitivity analysis

In this sub-section, we used a Partial Rank Correlation Coefficients (PRCC) adopted from previous works [36,49–53], to explore the sensitivity analysis of the autonomous type of the model (2.1), where the density-dependent public health education programs is assumed to be constant. The PRCC of the $\mathcal{R}_0$ and infection attack rate of the model (2.1) is depicted in Fig. 2 which reveals the effects of the model parameter on the $\mathcal{R}_0$ and the infection attack rate. We used 1000 random samples taken from uniform distributions of each model parameters from Table 2. For every random parameter sample set, the model was simulated to obtain the desired biological quantities.

6. Conclusions

This study used a classical SEIR-type model to study and analyze the transmission dynamics of typhoid fever disease, as well as to shed light on control and preventon mechanisms of the disease spreads in a population. The model is fitted using the yearly number of reported cases and demographic data relevant to typhoid fever dynamic in Taiwan. The main theoretical and epidemiological outcomes of this work are summarized as follows.

(i) Results of the basic reproduction number of the model with and without public health education program were determined analytically, which revealed that the basic reproduction number with public health education programs is less than or equal to the basic reproduction number without public health education programs indicating the impact of public health education programs for typhoid fever control and prevention. In addition, subsequent mathematical analysis results revealed that the DFE of the model is GAS whenever the basic reproduction number is less than or equals to 1, and unstable when the basic reproduction number is greater than unity. Further analytical result shows that the EE is GAS whenever the basic reproduction number is greater than unity, indicating the

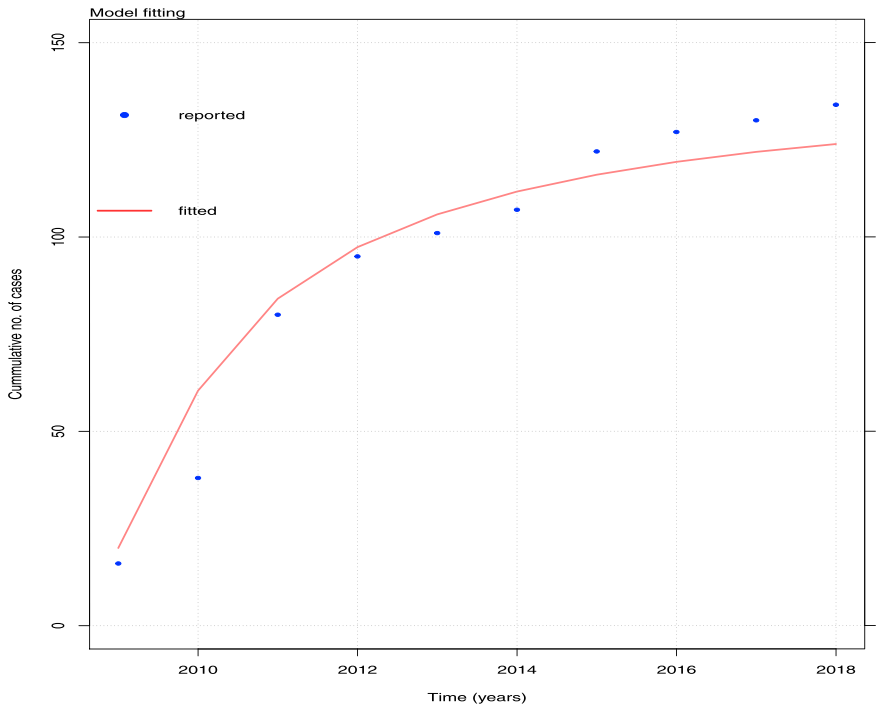

Fig. 1. Model fitting results using the biological parameter values given in Table 2 and the initial conditions given as: $S = 2000$, $I = 80$, $C = 20$, $R = 5$, $B = 2000$, and $A = 2$. The vertical axes denote the cumulative number of TP cases in Taiwan from 2009 to 2018.

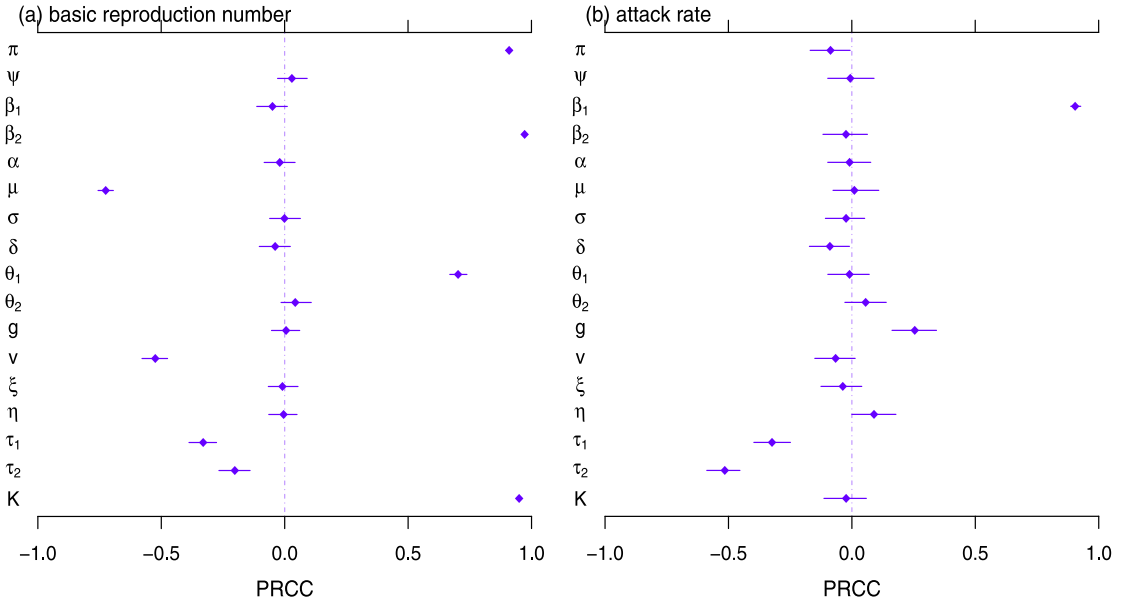

Fig. 2. Partial ranked correlation coefficients (PRCC) results for the sensitivity analysis obtained from the system (2.1). The dots denotes the PRCC estimation; and the bars are the 95% confidence intervals (CI). The baseline values of the model parameters are given in Table 2.

potential for the typhoid fever to spreads/persists in a population. Furthermore, the final size epidemic relation was computed for the reduced version of the model (2.1) (human-to-human transmission route only, i.e., model (4.1)) to report the approximate epidemic size over the cause of the typhoid epidemics.

(ii) Numerical simulations (data fittings), using the yearly number of reported typhoid fever cases in Taiwan during 2009–2018 period, shows that the model fitted well to the data, highlighting the usefulness of the model to predict a future scenario.

(iii) Sensitivity analysis of the model (using the basic reproduction number and infection attack rates as the two response functions) shows that the top three Partial Rank Correlation Coefficients ranked parameters are the half-saturation concentration of bacteria, the bacterial decay/removal rate, and infection rate from the environment to human. Hence, this study identifies the parameters that should be targeted for effective typhoid fever control in a community. Other parameters with high a PRCC ranking (but not as high as the most sensitive parameters) are the human death rate and recovery rate of typhoid from the carrier-class of humans.

(iv) Finally, the wavelets analysis is performed to examine the local periodicity of the typhoid cases data illustrated in Fig. B.1. Our results indicate a significant 1-year periodicity in the typhoid cases data.

Finally, this work employed an SEIR-based model to study and qualitatively analyzed the TF transmission dynamics in Taiwan, China and to shed light on the transmission of the TF epidemic with the effect of public health education programs. We also highlighted some vital epidemic parameters that should be emphasized for mitigation and control of TF epidemic in Taiwan, China. We noticed based on our results that environmental sanitation, public awareness campaigns, and provision of quality water supply are key factors to control the TP outbreaks, and can help to maintain TP transmission at a low level with minimal socio-economic disarray. Therefore, our results can have an important role in the public health for the design of sustainable policy that could generate a continuous and imperishable plan for controlling the TF outbreaks.

This study has some limitations, such as we plan to qualitatively analyze the non-autonomous version of the model; we plan to incorporate seasonality; finally, we plan to extend the model by incorporating an age-period-cohort model to find the best way to disseminate information about the TF outbreaks in population to timely and effectively prevent/control unexpected outbreaks in the future.

CRediT authorship contribution statement

Salihu Sabiu Musa: Conceptualization, Writing - original draft, Carried out the study. **Shi Zhao:** Carried out the study. **Nafiu Hussaini:** Writing - review & editing. **Salisu Usaini:** Writing - original draft. **Daihai He:** Conceptualization, Writing - original draft, Carried out the study.

Declaration of competing interest

The authors declare that they have no known competing financial interests or personal relationships that could have appeared to influence the work reported in this paper.

Availability of data and materials

All the data used in this work can be found in public domain.

Acknowledgments

The authors are grateful to the handling editor and reviewers for their helpful comments.

Funding

DH was supported by an Alibaba (China) Co. Ltd Collaborative Research grant (ZG9Z).

Appendix A. Proof of global stability analysis of the EE

Proof. Define a Lyapunov function as follows:

$$\begin{aligned} V(t) =& g_1(S - S^* - S^* \ln \frac{S}{S^*}) + g_1(I - I^* - I^* \ln \frac{I}{I^*}) + g_2(C - C^* - C^* \ln \frac{C}{C^*}) + \\ & g_3(B - B^* - B^* \ln \frac{B}{B^*}) + g_4(A - A^* - A^* \ln \frac{A}{A^*}). \end{aligned} \tag{A.1}$$

Thus, the Lyapunov derivative computed along solutions of the systems (2.1) is given by

$$\dot{V(t)} = g_1(1 - \frac{S^*}{S})\dot{S} + g_1(1 - \frac{I^*}{I})\dot{I} + g_2(1 - \frac{C^*}{C})\dot{C} + g_3(1 - \frac{B^*}{B})\dot{B} + g_4(1 - \frac{A^*}{A})\dot{A}. \tag{A.2}$$

Implies,

$$\begin{cases} \dot{V(t)} \leq g_1[\frac{-\mu_h(S-S^*)^2}{S}]+ \\ g_1\beta_1^*I^*S^*[1-\frac{\beta_1 IS}{\beta_1^*I^*S^*}-\frac{S^*}{S}+\frac{\beta_1 I}{\beta_1^*I^*}]+ \\ g_1\alpha\beta_1^*C^*S^*[1-\frac{\beta_1 CS}{\beta_1^*C^*S^*}-\frac{S^*}{S}+\frac{\beta_1 C}{\beta_1^*C^*}]+ \\ g_1\beta_2^*\frac{B^*S^*}{B^*+K}[1-\frac{\beta_2\frac{B}{B+K}S}{\beta_2^*\frac{B^*}{B^*+K}S^*}-\frac{S^*}{S}+\frac{\beta_2\frac{B}{B+K}}{\beta_2^*\frac{B^*}{B^*+K}}]+ \\ g_2\beta_1^*I^*S^*[\frac{\beta_1 IS}{\beta_1^*I^*S^*}-\frac{I}{I^*}-\frac{\beta_1 S}{\beta_1^*S^*}+1]+ \\ g_2\alpha\beta_1^*C^*S^*[\frac{\beta_1 CS}{\beta_1^*C^*S^*}-\frac{I}{I^*}-\frac{I^*\beta_1 CS}{I\beta_1^*C^*S^*}+1]+ \\ g_2\beta_2^*\frac{B^*}{B^*+K}S^*[\frac{\beta_2\frac{B}{B+K}S}{\beta_2^*\frac{B^*}{B^*+K}S^*}-\frac{I}{I^*}-\frac{I^*\beta_2\frac{B}{B+K}S}{I\beta_2^*\frac{B^*}{B^*+K}S^*}+1] \\ g_3\sigma I^*[\frac{I}{I^*}-\frac{C}{C^*}-\frac{C^*I}{CI^*}+1]+ \\ g_4\theta_1 I^*[\frac{I}{I^*}-\frac{B}{B^*}-\frac{B^*I}{BI^*}+1]+ \\ g_4\theta_2 C^*[\frac{C}{C^*}-\frac{B}{B^*}-\frac{B^*C}{BC^*}+1]+ \\ g_5\gamma A^*[2-\frac{A}{A^*}-\frac{A^*}{A}]. \end{cases} \tag{A.3}$$

Substituting $g_1=g_2=g_5=1$, $g_3=(\frac{S^*}{\sigma I^*})(\frac{\beta_2 B^*}{B^*+K}+\alpha\beta_1^*C^*)$, and $g_4=\frac{\beta_1^*S^*}{\theta_1}$, (and the fact that the arithmetic mean is greater than or equal to the geometric mean [54,55]), we have

$$\begin{cases} \dot{V(t)} \leq \beta_1^*I^*S^*[2-\frac{S^*}{S}-\frac{I}{I^*}-\frac{\beta_1 S}{\beta_1^*S^*}+\frac{\beta_1 I}{\beta_1^*I^*}]+ \\ \alpha\beta_1^*C^*S^*[2-\frac{S^*}{S}-\frac{I}{I^*}-\frac{\beta_1 SI^*C}{\beta_1^*S^*IC^*}+\frac{\beta_1 C}{\beta_1^*C^*}]+ \\ \beta_2^*\frac{B^*S^*}{B^*+K}[2-\frac{S^*}{S}-\frac{I}{I^*}-\frac{\beta_2 SI^*\frac{B}{B+K}}{\beta_2^*S^*I\frac{B^*}{B^*+K}}+\frac{\beta_2\frac{B}{B+K}}{\beta_2^*\frac{B^*}{B^*+K}}]+ \\ (\frac{S^*}{\sigma I^*})(\frac{\beta_2 B^*}{B^*+K}+\alpha\beta_1^*C^*)\sigma I^*[\frac{I}{I^*}-\frac{C}{C^*}-\frac{C^*I}{CI^*}+1]+ \\ \beta_1^*S^*I^*[\frac{I}{I^*}-\frac{B}{B^*}-\frac{B^*I}{BI^*}+1]+ \\ \frac{\theta_2}{\theta_1}\beta_1^*S^*C^*[\frac{C}{C^*}-\frac{B}{B^*}-\frac{B^*C}{BC^*}+1]. \end{cases} \tag{A.4}$$

Note that by direct calculation, and using condition (3.8), we have that:

$$\begin{aligned} &[2-\frac{S^*}{S}-\frac{I}{I^*}-\frac{\beta_1 S}{\beta_1^*S^*}+\frac{\beta_1 I}{\beta_1^*I^*}]= \\ &[-(1-\frac{\beta_1 I}{\beta_1^*I^*})(1-\frac{B\beta_1^*I^*}{B^*\beta 1I})+3-\frac{S^*}{S}-\frac{\beta S}{\beta_1^*S^*}-\frac{B\beta_1^*I^*}{B^*\beta_1 I}-\frac{I}{I^*}+\frac{B}{B^*}]\leq \\ &-(\frac{S^*}{S}-1)-(\frac{\beta_1 S}{\beta^*S^*}-1)-(\frac{B\beta_1^*I^*}{B^*\beta_1 I})-\frac{I}{I^*}+\frac{B}{B^*}= \\ &[-\ln(\frac{S^*}{S}\frac{\beta_1 S}{\beta_1^*S^*}\frac{B\beta_1^*I^*}{B^*\beta_1 I})-\frac{I}{I^*}+\frac{B}{B^*}]=[\frac{B}{B^*}-\ln(\frac{B}{B^*})-\frac{I}{I^*}+\ln(\frac{I}{I^*})]. \end{aligned} \tag{A.5}$$

Similarly, using condition (3.9), we have

$$[2-\frac{S^*}{S}-\frac{I}{I^*}-\frac{\beta_1 SI^*C}{\beta_1^*S^*IC^*}+\frac{\beta_1 C}{\beta_1^*C^*}]\leq[\frac{C}{C^*}-\ln(\frac{C}{C^*})-\frac{I}{I^*}+\ln(\frac{I}{I^*})] \tag{A.6}$$

And also, using condition (3.10), we have

$$[2-\frac{S^*}{S}-\frac{I}{I^*}-\frac{\beta_2 SI^*\frac{B}{B+K}}{\beta_2^* S^* I\frac{B^*}{B^*+K}}+\frac{\beta_2\frac{B}{B+K}}{\beta_2^*\frac{B^*}{B^*+K}}]\leq[\frac{C}{C^*}-\ln(\frac{C}{C^*})-\frac{I}{I^*}+\ln(\frac{I}{I^*})]. \tag{A.7}$$

Following [27,50,54,56,57], the function $v(x)=1-x+\ln x$, then, if $x>0$ it leads to $v(x)\leq 0$. And if $x=1$, $v(x)=0$, so that $x-1\geq\ln(x)$ for any $x>0$. Thus, we have

$$\begin{cases}\dot{V}(t)\leq\beta_1^* I^* S^*[\frac{B}{B^*}-\ln(\frac{B}{B^*})-\frac{I}{I^*}+\ln(\frac{I}{I^*})]+\\ \alpha\beta_1^* C^* S^*[\frac{C}{C^*}-\ln(\frac{C}{C^*})-\frac{I}{I^*}+\ln(\frac{I}{I^*})]+\\ \beta_2^*\frac{B^*S^*}{B^*+K}[\frac{C}{C^*}-\ln(\frac{C}{C^*})-\frac{I}{I^*}+\ln(\frac{I}{I^*})]+\\ \beta_2^*\frac{B^*S^*}{B^*+K}[\frac{I}{I^*}-\ln(\frac{I}{I^*})-\frac{C}{C^*}+\ln(\frac{C}{C^*})]+\\ \alpha\beta_1^* C^* S^*[\frac{I}{I^*}-\ln(\frac{I}{I^*})-\frac{C}{C^*}+\ln(\frac{C}{C^*})]+\\ \beta_1^* I^* S^*[\frac{I}{I^*}-\ln(\frac{I}{I^*})-\frac{B}{B^*}+\ln(\frac{B}{B^*})]+\\ \beta_1^* C^* S^*(\frac{\theta_2}{\theta_1})[\frac{C}{C^*}-\ln(\frac{C}{C^*})-\frac{B}{B^*}+\ln(\frac{B}{B^*})].\end{cases} \tag{A.8}$$

Hence, the conditions (3.8)–(3.10) and (A.1)–(A.8) ensure that $\frac{dV}{dt}\leq 0$ provided that $\frac{C}{C^*}-\ln\frac{C}{C^*}\leq\frac{B}{B^*}-\ln\frac{B}{B^*}$. Furthermore, the strict inequality $\frac{dV}{dt}=0$ holds only for $S=S^*$, $I=I^*$, $C=C^*$, $R=R^*$, $B=B^*$, $A=A^*$. Thus, the E^* (i.e., EE state) is the only positive invariant set to the system (2.1) contained entirely in

$$\left\{(S,I,C,R,B,A)\in\Omega : S=S^*, I=I^*, C=C^*, R=R^*, B=B^*, A=A^*\right\}.$$

Hence, it follows from the *LaSalle's* invariance principle [41] that every solutions to the equations in (A.8) with initial conditions in Ω converge to E^*, as $t\to\infty$. Therefore, the (positive) EE, E^*, is GAS.

Appendix B. Wavelets analysis

In order to examine the local periodicity of the typhoid cases data, a wavelet analysis adopted from [31,58,59] was performed, and depicted in Fig. B.1. The red regions indicate significant periodicities. We fixed the base wavelet, $u(t)$, to be the Morlet wavelet. The wavelet transformation is given by $Z_{u,\phi_1}(\phi_2,\phi_3)=\int_{-\infty}^{\infty}\phi_1(t)\cdot u^*_{\phi_2,\phi_3}(t)\,dt$. The term Z represents the wavelet coefficient, which represents the contribution of each base wavelets (u) with given wavelet scale

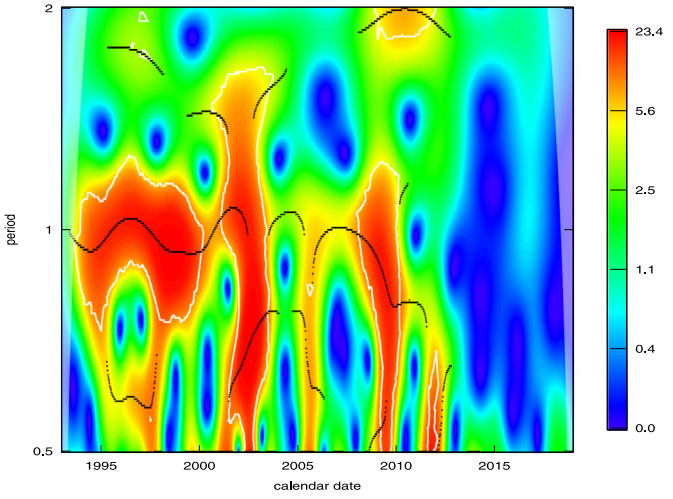

Fig. B.1. The power spectra for the wavelet periodicity in the typhoid cases time series. The red regions represents dominant periodicity, and blue denotes low levels of inferred periodicity. (For interpretation of the references to color in this figure legend, the reader is referred to the web version of this article.)

(ϕ_2) and the time position (ϕ_3). The function $\phi_1(t)$ denotes the time series of typhoid fever outbreaks, while the term u^* denotes the complex conjugation of the base wavelet (u). Hence, the wavelet reconstruction can be calculated by the linear combination of each pair of $Z(\phi_2, \phi_3)$ and u_{ϕ_2,ϕ_3}.

References

[1] World Health Organization. Typhoid fact sheet. 2019, Available from https://www.who.int/news-room/fact-sheets/detail/typhoid or https://www.who.int/immunization/diseases/typhoid/en/ [Accessed 2019].
[2] Mushayabasa S. Modeling the impact of optimal screening on typhoid dynamics. Int J Dyn Control 2016;4(3):330–8.
[3] Mutua JM, Wang F, Vaidy NK. Modeling malaria and typhoid fever co-infection dynamics. Math Biosci 2015;264:128–44.
[4] Anderson RM, May RM. Infectious diseases of humans: dynamics and control. Oxford: Oxford University Press; 1991.
[5] Capasso V, Serio G. A generalization of the kermack-mckendrick deterministic epidemic model. Math Biosci 1978;42(1–2):43–61.
[6] Garba SM, Gumel AB, Bukar MRA. Backward bifurcations in dengue transmission dynamics. Math Biosci 2008;215(1):11–25.
[7] Hethcote HW. Qualitative analysis of communicable disease models. Math Biosci 1976;28:335–56.
[8] Kermack WO, McKendrick AG. Contributions to the mathematical theory of epidemics, part I. Proc R Soc Ser A 1927;115(5):700–21.
[9] Kermack WO, McKendrick AG. Contributions to the mathematical theory of epidemics, part II. Proc R Soc Ser A 1932;138:55–83.
[10] Wang W, Zhao XQ. Threshold dynamics for compartmental epidemic models in periodic environments. J Dyn Differential Equations 2008;20:699–717.
[11] Yorke JA, London WP. Recurrent outbreaks of measles, chickenpox and mumps: II. systematic differences in contact rates and stochastic effects. Am J Epidemiol 1937;98(6):469–82.
[12] Ferguson N. Capturing human behaviour. Nature 2007;446(7137):733.
[13] Funk S, Gilad E, Jansen VA. Endemic disease, awareness, and local behavioural response. J Theoret Biol 2010;264(2):501–9.
[14] Funk S, Salathe M, Jansen VA. Modelling the influence of human behaviour on the spread of infectious diseases: a review. J R Soc Interface 2010;7:1247–56.
[15] Wang XX, Gao D, Wang J. Influence of human behavior on cholera dynamics. Math Biosci 2015;267:41–52.
[16] Abdelrazec A, Belair J, Shan C, Zhu H. Modeling the spread and control of dengue with limited public health resources. Math Biosci 2016;271:136–45.
[17] He D, Wang X, Gao D, Wang J. Modeling the 2016-2017 yemen cholera outbreak with the impact of limited medical resources. J Theoret Biol 2018;451:80–5.
[18] Shan C, Yi Y, Zhu H. Nilpotent singularities and dynamics in an SIR type of compartmental model with hospital resources. J Differential Equations 2016;260(5):4339–65.
[19] Shan C, Zhu H. Bifurcations and complex dynamics of an SIR model with the impact of the number of hospital beds. J Differential Equations 2014;257(5):1662–88.
[20] Wang A, Xiao Y, Zhu H. Dynamics of a filippov epidemic model with limited hospital beds. Math Biosci Eng 2018;15(3):739–64.
[21] Zhou L, Fan M. Dynamics of an SIR epidemic model with limited medical resources revisited. Nonlinear Anal: Real World Appl 2012;13(1):312–24.
[22] Funk S, Gilad E, Watkins C, Jansen VA. The spread of awareness and its impact on epidemic outbreaks. Proc Natl Acad Sci 2009;106(16):6872–7.
[23] Hussaini N, Winter M, Gumel AB. Qualitative assessment of the role of public health education program on HIV transmission dynamics. Math Med Biol 2011;28(3):245–70.
[24] Kaur N, Ghosh M, Bhatia SS. Modeling and analysis of an SIRS epidemic model with effect of awareness programs by media. Int J Math Comput Phys Quant Eng 2014;8(1):233–9.
[25] Li J, Ma M. The analysis of a drug transmission model with family education and public health education. Infect Dis Model 2018;3:74e84.
[26] Misra AK, Sharma A, Shukla JB. Modeling and analysis of effects of awareness programs by media on the spread of infectious diseases. Math Comput Model 2011;53(5–6):1221–8.
[27] Yang C, Wang X, Gao D, Wang J. Impact of awareness programs on cholera dynamics: two modeling approaches. Bull Math Biol 2017;79(9):2109–31.
[28] Zuo L, Liu M. Effect of awareness programs on the epidemic outbreaks with time delay. Abstr Appl Anal 2014;940841, 8 pages.
[29] Mushayabasa S. Impact of vaccines on controllong typhoid fever in kassena-nenkana district of upper east region of ghana: Insights from a mathematical model. J Modern Math Stat 2011;5(2):54–9.
[30] Mushayabasa S, Bhunu CP, Mhlanga NA. Modeling the transmission dynamics of typhoid in malaria endemic settings. Appl Appl Math 2014;9(1):121–40.
[31] Musa SS, Zhao S, He D, Liu C. The long-term periodic patterns of global rabies epidemics among animals: A modeling analysis. Int J Bifurcation Chaos 2020;30(03):2050047.
[32] Lakshmikantham V, Leela S, Martynyuk AA. Stability analysis of nonlinear systems. New York and Basel: Marcel Dekker Inc; 1989.
[33] Hussaini N, Okuneye K, Gumel AB. Mathematical analysis of a model for zoonotic visceral leishmaniasis. Infect Dis Model 2017;2(4):455–74.
[34] Usaini S, Mustapha UT, Musa SS. Modelling scholastic underachievement as a contagious disease. Math Methods Appl Sci 2018;41:8603–12.
[35] Diekmann O, Heesterbeek JAP, Metz JAJ JAJ. On the definition and the computation of the basic reproduction ratio R0 in models for infectious diseases in heterogeneous populations. J Math Biol 1990;28(4):365–82.
[36] Musa SS, Zhao S, Gao D, Lin Q, Chowell G, He D. Mechanistic modelling of the large-scale lassa fever epidemics in Nigeria from 2016 to 2019. J Theoret Biol 2020;493:110209. http://dx.doi.org/10.1016/j.jtbi.2020.110209.
[37] van den Driessche P, Watmough J. Reproduction numbers and sub-threshold endemic equilibria for compartmental models of disease transmission. Math Biosci 2002;180(1–2):29–48.
[38] Musa SS, Qureshi S, Zhao S, Yusuf A, Mustapha UT, He D. Mathematical modeling of COVID-19 epidemic with effect of awareness programs. Infect Dis Model 2021;6:448–60.
[39] Baba IA, Yusuf A, Nisar KS, Abdel-Aty AH, Nofal TA. Mathematical model to assess the imposition of lockdown during COVID-19 pandemic. Results Phys. 2021;20:103716.
[40] Gao D, Ruan S. An SIS patch model with variable transmission coefficients. Math Biosci 2011;232(2):110–5.
[41] LaSalle JP. The stability of dynamical systems. Regional conference series in applied mathematics, Philadelphia: SIAM; 1976.
[42] Thieme HR. Persistence under relaxed point-dissipativity (with application to an endemic model). SIAM J Math Anal 1993;24(2):407–35.
[43] Arino J, Brauer F, van den Driessche P, Watmough J, Wu J. A final size relation for epidemic models. Math Biosci Eng 2007;4(2):159–75.
[44] Barbarossa MV, De'nes A, Kiss G, Nakata Y, Rost G, Vizi Z. Transmission dynamics and final epidemic size of ebola virus disease outbreaks with varying interventions. PLoS One 2015;10(7):e0131398.
[45] Misra AK, Gupta A, Venturino E. Cholera dynamics with bacteriophage infection: a mathematical study. Chaos Solitons Fractals 2016;91:610–21.

[46] Taiwan National Infectious Disease Statistics System. Typhoid fever. 2019, Available from: https://nidss.cdc.gov.tw/en/SingleDisease.aspx?dc=1&dt=2&disease=002 [Accessed 2020].
[47] World Bank Data. World bank data population website. 2019, http://data.isdb.org/pxfdrcg/world-bank-development-indicators-wdi-2017-idb-aggregates?tsId=1077410 [Accessed 2019].
[48] Geoba.se, population website. 2020, Available from: http://www.geoba.se/country.php?cc=TW&year=2018. [Accessed August, 2020].
[49] Gao D, Lou Y, He D, Porco TC, Kuang Y, Chowell G, Ruan S. Prevention and control of zika as a mosquito-borne and sexually transmitted disease: a mathematical modeling analysis. Sci Rep 2016;6:28070.
[50] Musa SS, Zhao S, chan HS, Jin Z, He D. A mathematical model to study the 2014-2015 large-scale dengue epidemics in kaohsiung and tainan cities in Taiwan, China. Math Biosci Eng 2019;16(5):3841–63.
[51] Xiao Y, Tang S, Wu J. Media impact switching surface during an infectious disease outbreak. Sci Rep 2015;5:7838.
[52] Zhao S, Lou Y, Chiu AP, He D. Modelling the skip-and-resurgence of Japanese encephalitis epidemics in Hong Kong. J Theor Biol 2018;454:1–10.
[53] Zhao S, Stone L, Gao D, He D. Modelling the large-scale yellow fever outbreak in luanda, angola, and the impact of vaccination. PLoS Negl Trop Dis 2018;12(1):e0006158.
[54] Sun G, Xie J, Huang S, Jin Z, Li M, Liu L. Transmission dynamics of cholera: mathematical modeling and control strategies. Commun Nonlinear Sci Numer Simul 2017;45:235–44.
[55] Roop OP, Chinviriyasit W, Chinviriyasit S. The effect of incidence function in backward bifurcation for malaria model with temporary immunity. Math Biosci 2015;265:47–64.
[56] Lin Q, Musa SS, Zhao S, He D. Modeling the 2014-2015 ebola virus disease outbreaks in sierra leone, guinea, and liberia with effect of high- and low-risk susceptible individuals. Bull Math Biol 2020;82(102). http://dx.doi.org/10.1007/s11538-020-00779-y.
[57] Shuai Z, van den Driessche P. Global stability of infectious disease models using Lyapunov functions. SIAM J Appl Math 2013;73(4):1513–32.
[58] Cazelles B, Chavez M, Berteaux D, Me'nard F, Olav Vik J, Jenouvrier S, Stenseth NC. Wavelet analysis of ecological time series. Oecologia 2008;156:287–304.
[59] Tang X, Zhao S, Chiu APY, Wang X, Yang L, He D. Analysing increasing trends of guillain-barre syndrome (GBS) and dengue cases in Hong Kong using meteorological data. PLoS One 2017;12:e0187830.